British Journal of Applied Science & Technology
3(4): 1228-1245, 2013

SCIENCEDOMAIN *international*
www.sciencedomain.org

Effect of Sodium Carboxymethyl Cellulose Concentration on the Photophysical Properties of Zinc Sulfide Nanoparticles

I. Ahemen[1*], O. Meludu[2] and E. Odoh[2]

[1]Department of Physics, University of Agriculture Makurdi, Nigeria.
[2]Department of Physics, Modibbo Adama University of Technology Yola, Nigeria.

Authors' contributions

This work was carried out in collaboration between all authors. Author IA designed the study in collaboration with author OM, performed the experiments and wrote the first draft. Authors OM and EO read the manuscript and made useful suggestions. They both contributed in the analysis of the results. All authors read and approved the final manuscript.

Research Article

Received 17th March 2013
Accepted 23rd July 2013
Published 9th August 2013

ABSTRACT

The effect of sodium carboxymethyl cellulose (CMC) as capping agent on the optical (photo) and structural (physical) properties of zinc sulfide (ZnS) nanoparticles was studied. The capped nanoparticles were grown by the precipitation technique. The capping ratio of precursor (ZnS) to surfactant (CMC) (vol/vol) considered were 1:1 (sample S_1), 1:2 (S_2 sample) and 1:3 (sample S_3 sample). Analyses carried out include; X-ray diffraction (XRD), scanning electron microscopy (SEM), fourier transform infrared spectroscopy (FTIR), UV-Vis spectroscopy and photoluminescence studies. SEM analysis revealed particles as agglomerates. The obtained band gap energies of 4.13, 4.20 and 4.27 eV for samples S_1, S_3 and S_2, respectively are blue shifted when compared to the band gap energy of bulk ZnS semiconductor indicating quantum effect. The calculated particle sizes from XRD (3.14, 3.73 and 15.7 nm for samples S_3, S_2 and S_1, respectively) and effective mass approximation (3.59, 3.77 and 3.98 nm for samples S_2, S_3 and S_1, respectively) were found to vary with the capping amount, though not monotonically. Capping ZnS with higher amount of CMC provided more stable nanoparticles, although with lower luminescence. The emission peaks of samples S_3 and S_2 were red-shifted when compared to that of sample S_1. At low CMC capping amount, the luminescence was found to be very high and blue shifted due to a greater

**Corresponding author: E-mail: ahemior@gmail.com;*

participation of surface trap states.

Keywords: Zinc sulfide; sodium carboxymethyl cellulose; nanoparticles; stability; surface.

1. INTRODUCTION

The growing interest in the study of semiconductor materials at nanoscale is primarily because of the unique photophysical properties associated with semiconductors in this small size regime. Semiconductor nanocrystallites such as ZnS have their optical properties like absorption and luminescence changed from their bulk counterpart through quantum confinement effect. As the size of the semiconductor is reduced to a size comparable to its exciton Bohr radius, changes in the electronic structure and physical properties occur [1]. These changes include; stoke shift of energy, discretization of energy spectra, concentration of the oscillator strength, geometrical confinement of phonons and increase in surface effect [1].

Zinc sulfide (ZnS) nanocrystals have also been studied extensively because of their potential application in electronic devices such as flat panel displays, light emitting diodes, thin film electroluminescence devices, photocalysis and as window materials [2,3]. Some of the properties that make ZnS semiconductor a promising material in optoelectronics devices are its wide band gap (3.6 eV), the relatively good chemical and photo stability, and low toxicity of the semiconductor when compared to other chalcogenides like CdS, CdSe and CdTe [4-6]. At room temperature ZnS stabilizes as cubic (zinc blende) structure, but transforms into wurzite structure when synthesized at elevated temperatures. Another promising property of ZnS is the ability to engineer the band gap in order to tune its optoelectronic properties. By varying ZnS particle size, blue and white emissions have been obtained [2,7]. However, because of large-surface-to-volume ratio of these small nanocrystallites, surface related recombination may become dominant and reduce the luminescence (or quantum) efficiency of the nanoparticles significantly [8-10]. Also, apart from surface effect, Ostwald ripening and Vander-Waals interactions between particles could lead to agglomeration of small particles into larger particles if the synthesis process does not involve capping agents [10].

One way of reducing surface effects and reducing particles agglomeration is through nanoparticles surface passivation (or capping) with organic or inorganic molecules [11]. The choice of the capping molecule is critical. The bonding between the capping molecule and nanocrystals precursor need to be neither too weak nor too strong [12]. Weak bonding triggers fast particle growth and larger crystallites, while strong bonding may not form nanocrystals [12]. Thus, the nature of capping molecules, temperature of reaction, the dynamics of attaching and de-attaching of nanocrystals and surfactant complexes, and the concentration of the capping molecules are critical to obtaining the desired nanoparticles [12].

Several organic materials have been used to sterically and electrostatically stabilize nanoparticles against agglomeration and formation of surface defect sites or traps. These polymer materials include polyvinyl alcohol [13,14], hexadecylamine [15], Oleic acid [9], thioglycerol [16], polyethylene glycol [17], polyvinyl pyrrolidone and thioglycolic acid [9,18], methacrylic acid [19], Styrene butadiene rubber latex – SBR [20] and sodium carboxymethyl cellulose [21,22].

Sodium carboxymethyl Cellulose (CMC) is obtained by activation of cellulose with aqueous NaOH in a slurry of an aqueous organic solvent followed by reacting the cellulose with monochloroacetic acid. The functional properties of CMC depend on the degree of substitution of cellulose backbone structure and the degree of carboxymethyl substituents [23]. CMC has high transparency [22], is low cost and environmentally friendly [24] and so when used as a capping material will help reduce the potential for toxicity. The presence of both carboxylated and hydroxyl groups makes CMC to readily form complexation with divalent alkaline metals. The higher molecular weight and a net negative surface charge of CMC have been utilized to stabilize nanoparticles against agglomeration through steric hindrance and electrostatic stabilization [21,22]. CMC-copper complexes have also been prepared as paper additive and were found to enhance durability and strength properties of pulp paper sheet [22]. In this paper, we report the effect of concentration of sodium carboxymethyl cellulose (CMC) on the structural and optoelectronic properties of ZnS (i.e. ZnS/CMC) nanoparticles.

2. MATERIALS AND METHODS

2.1 Synthesis of ZnS Nanocrystals Capped with Different Amounts of CMC

In the present work, 1g of CMC was put into a beaker containing 90 ml of deionized water and allowed to dissolve at room temperature until a clear solution was formed. The solution was then made up to 100 ml by adding more deionized water. 25 ml of (0.2M) $ZnSO_4.7H_2O$ was mixed with 1:1, 1:2 and 1:3 (vol/vol) ratios (named S_1, S_2 and S_3, CMC respectively) of CMC. The pH of this mixture was adjusted to 4.0 using acetic acid. 0.2M of $Na_2S.\ 9H_2O$ was drop-wise added to the mixed solution (with continuous stirring) at room temperature. The mixture was kept under stirring for another 15 min after the last drop of $Na_2S.\ 9H_2O$ was added for complete mixing of species.

The white precipitate obtained was centrifuged at 3500 revolutions per minutes for 20 minute and washed several times with a mixture of toluene and ethanol solution. This was followed by filtration to obtain white solid ZnS/CMC nanoparticles. The solid particles were dried in a vacuum oven at 90ºC for 6 hours and then made into fine powder by grinding. The synthesized nanoparticles were stored for six months before characterization. The powders of samples S_1, S_2 and S_3 were then characterized using UV-Visible spectroscopy (JENWAY 6405 at EMDI Akure, Nigeria), Scanning Electron Microscope (Carl-Zeiss at SHESTCO Abuja, Nigeria and Center for Nanostructured materials Pretoria, South Africa), Transmission Electron Microscopy (TEM) and High Resolution Transmission Microscopy (HRTEM) (JEOL-JEM 2100 TEM facility at the Center for Nanostructured materials Pretoria, South Africa) Fourier transform Infrared Spectroscope (Shimadzu-IR 4800s), X-ray Diffraction (PANalytic X'Pert PRO at SHESTCO Abuja, Nigeria) and Photoluminescence analysis (using Jobin Yvon monochromator equipped with a pulse laser excitation source and ICCD camera detection) at Laboratorire de Chimie de la Matière Condensee de Paris, France.

3. RESULTS AND DISCUSSION

3.1 Crystal Structure and Size Determination

In Fig. 1 is shown the XRD diffractograms for (a) S_1, (b) S_2 and (c) S_3 nanoparticles (NPs), respectively. Sample S_1, which is ZnS capped with sodium carboxymethyl cellulose at 1:1 (vol/vol) of precursor to surfactant, have broader diffraction peaks characteristics of

nanoparticles (Fig. 1a). The diffraction peaks can be indexed to the mixed cubic and hexagonal phase of ZnS. The diffraction peaks (2θ) at 28.0632º, 47.5652º and 56.3377º corresponding to d-spacing of 3.1480 nm, 1.8639 nm and 1.5531 nm, respectively are identified to originate from (111), (220) and (311) planes of the cubic (zinc blende) phase of ZnS (ICDD reference number 00-001-0792 or JCPDS No. 05-0566). The other diffraction peaks may be coming from the oxidation/degradation of the components of the sample. In the nanoparticles stabilization process, the presence of carboxylate (- COO-) and hydroxyl (-OH) functional groups in CMC provides a net negative surface charge which ensure nanocrystals (NCs) stability through electrostatic interaction. Therefore, with higher amount of CMC in the ZnS NPs formation, there is higher electrostatic interaction between NPs and CMC leading to well stabilized NPs. At low amount of CMC the number of carbonyl and hydroxyl groups available for complexation is decreased, allowing more ZnS NPs to interact with each other and the environment. Also, steric hindrances dominate in limiting particles growth at this low CMC concentration; unfortunately, this may not be very effective in the stabilization process. The poor particles stabilization could lead to faster degradation of the NPs as can be observed in Fig. 1(a) with the emergence of peaks at 17.2135º, 19.0794º, 23.2002º, 29.0274º, 32.8787º, 33.8803, 37.6414º and 42.3012º. These peaks could be coming from the oxidation of ZnS into its constituents like $Zn(OH)_2$, ZnO, $ZnSO_4$ and absorbed water. For example the peaks at 32.8787º, 33.8803 and 37.6414º can be indexed to (100), (002) and (101) planes of ZnO [11,25,26].

Similarly, the diffraction pattern of sample S_2 (Fig. 1b) has (2θ) peaks positioned at 28.7536º, 47.6318º, 56.1381º corresponding to d-spacing of 3.1339 nm, 1.9092 nm and 1.6076 nm respectively. These peaks are also identified to originate from (111), (220) and (311) planes of the zinc blende structure of ZnS (JCPDS No. 05-0566). The extraneous peaks are located at the same position as those found in S_1 sample pattern. The peaks are fewer in number and have lower intensity variations. The reason may be that the increase in amount of CMC in sample S_2 provided better coordination and stability of the nanoparticles surface. The XRD diffraction pattern of S_3 (Fig. 1c) shows that the nanocrystals have their diffraction peaks located at the 2θ angles of 28.5144º, 47.4650º and 56.1883º corresponding to d-spacing of 3.2281 nm, 1.8715 nm and 1.5345 nm respectively. These peaks are also assigned to the (111), (220) and (311) planes of the cubic structure of ZnS (JCPDS No. 05-0566). Most of the extraneous peaks found in the XRD patterns of S_1 sample have almost vanished in sample S_3 due to better complexation of all the Zn^{2+} by the available carboxylic groups in the CMC. The three major diffraction peaks are less broadened with lower intensity variations, which may account for better stability.

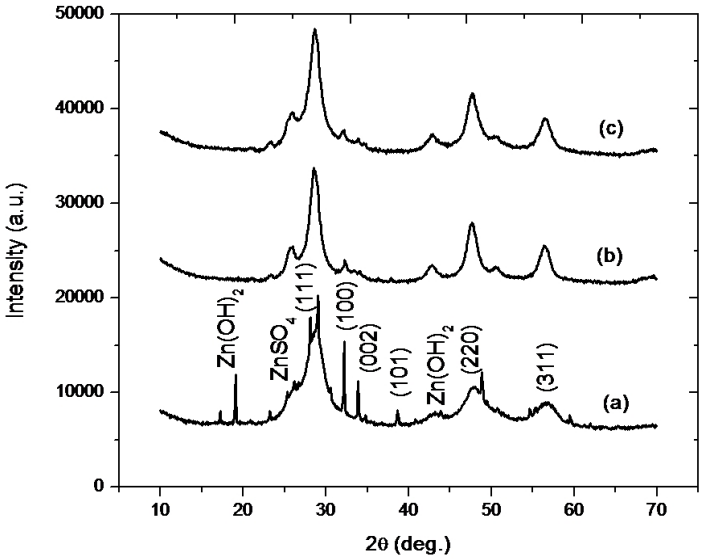

Fig. 1. XRD pattern of (a) S_1, (b) S_2, (c) S_3

The calculated lattice constants using the values of d-spacing for the (111) plane are in good agreement with the standard lattice constant of bulk ZnS with d-spacing of 3.1230 nm (a = 0.540 nm) [27]. The broadening of the diffraction peaks is an indication that the synthesized ZnS semiconductors have particles with dimension in the nanometer scale [17]. The average crystallite size was estimated from the average of the crystallite sizes obtained from each of the (111), (220), (311) diffraction peaks for all the samples (Table 1). In addition to these sizes, average crystal size were obtained by averaging the sizes evaluated from each of the (001), (002), (101) diffraction peaks of sample S_1 using the Debye-Scherrer formula (equation 1) [28]:

$$D_{hkl} = \frac{k\lambda}{\beta Cos\theta} \tag{1}$$

where D = average crystallite size perpendicular to crystallographic orientation (hkl); β is the full width at half-maximum (FWHM) of the (hkl) crystal face diffraction peaks; λ is the wavelength of X-ray radiation (0.154060 nm); θ is the Bragg diffraction angle of (hkl) crystal face; K is a constant with values between 0.89 to 1 depending on the crystal symmetry; 0.94 for FWHM of integral breadth of spherical crystals with wurzite or cubic symmetry.

The calculated crystallite size gave a distribution of small crystals [average size of 2.31 nm] from the (111), (220) and (331) diffraction planes] and larger crystals [average size of 27.9 nm from (001), (002) and (101) reflections] for sample S_1. Therefore, the average crystal size for both the small and large crystals is 15.7 nm. Clearly, this result suggests a systematic decrease in the average crystal size with increase in the CMC concentration which is consistent with the trend of particle sizes obtained from SEM and TEM (Table 1). Suppression of the extraneous diffraction peaks in samples S_2 and S_3 suggests better stability for ZnS nanoparticles capped at higher CMC concentration. Also, the smaller

average crystal size distribution obtained for these samples is an indication that at higher CMC concentrations, steric hindrances were more effective in restricting particle growth and agglomeration. The fact that particles capped with larger amount of CMC provided more stability with smaller average crystal size distribution agrees with the report by Sakulchaicharoen et al. [21] that more stable nanocomposites are formed through electrostatic stabilization while particles growth is controlled by steric hindrance (density or molecular weight of CMC).

Table 1. Calculated band gap energies, stoke shift, crystallite size (Scherrer formula) and particle size (EMA) of ZnS/CMC samples

Sample	Band-gap Energy , *eV*	Energy Stoke Shift, *eV*	Average Crystal size (XRD), nm	Average Particles size (TEM), nm	Particles size (SEM), nm	Particle size (EMA), nm
S_1	4.13	0.53	15.7	6.7	163	3.98
S_2	4.27	0.67	3.73	4.7	85	3.59
S_3	4.20	0.60	3.14	4.1	43	3.77

3.2 Morphological and Elemental Characterization

3.2.1 SEM and EDX analysis

Fig. 2(a) is the SEM image of the CMC used in this work. The CMC molecules are rod-like (or ribbon shaped) which is similar to other reported images for a typical CMC molecule [29,30]. The results in Fig. 2(b), Fig. 2(c) and Fig. 2(d) show agglomerates of ZnS nanoparticles embedded in the CMC matrix. The result of the average particle sizes obtained from SEM images shows that indeed the particles were agglomerates with their sizes decreasing with increase CMC concentration. At higher CMC concentration, electrostatic potential at the CMC surface restricts ZnS nanoparticles from interacting with each other and forming larger agglomerates. The number of carbonyl group present in the CMC solution is sufficient to cause better dispersion of the nanoparticles in the CMC matrix. The smooth surface observed in the respective micrographs suggests that CMC act as a good passivating agent during ZnS synthesis.

The elemental composition of both raw CMC and CMC-capped ZnS nanoparticles are shown in the EDX spectra (Fig. 3a and 3b). From the spectrum in Fig. 3(b), CMC can be seen to be composed of carbon, oxygen, sodium, gold, chlorine and aluminium. The gold is most likely coming from the gold grid used in holding the sample. In Fig. 3(a), the peaks at 1.0 KeV, and 8.6 KeV correspond to the transition of zinc (Zn) while the peak at 2.4 KeV correspond to the transition of the sulfide (S) indicating ZnS embedded in the CMC matrix. The Na^+ found in Fig. 3(a) shows that Na^+ ions were not completely displaced by the Zn^{2+} ions in the reaction.

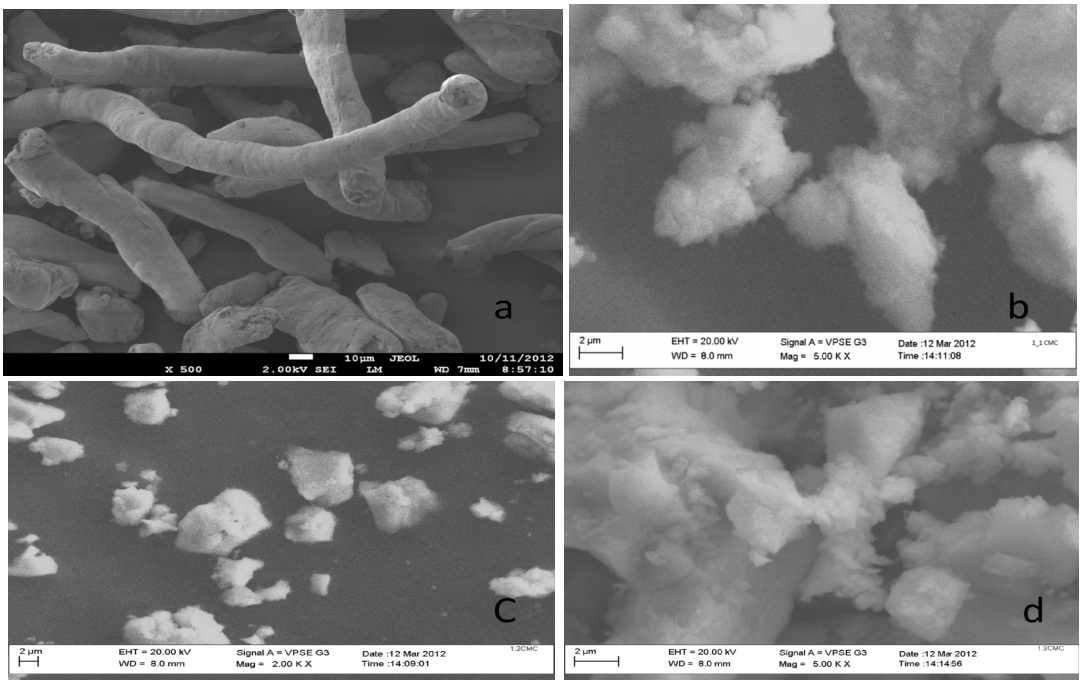

Fig. 2. SEM micrographs of (a) CMC, (b) S_1, (c) S_2 and (d) S_3 samples.

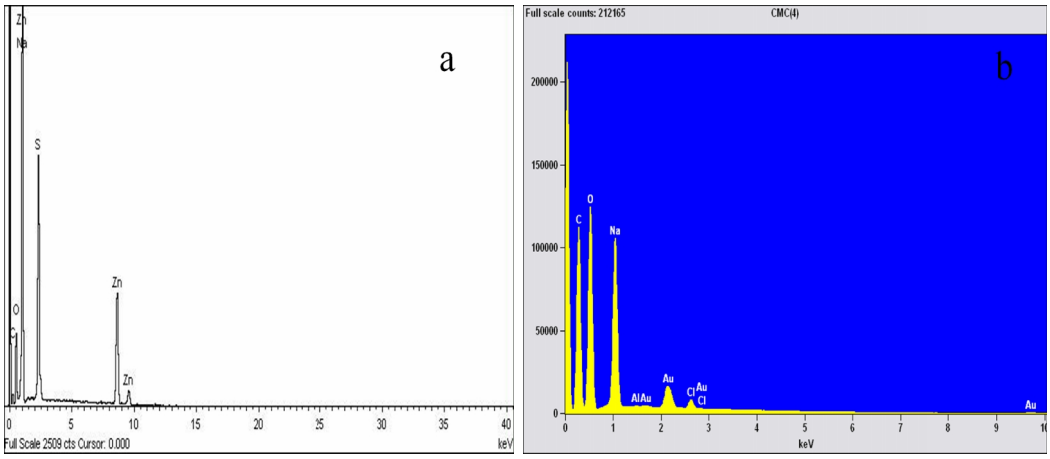

Fig. 3. EDX spectra of (a) ZnS capped with CMC and (b) typical raw CMC used in this work

3.2.2 TEM – HRTEM analysis

Fig. 4 show the TEM and HRTEM images of sample S_1.The TEM image in Fig. 4a reveals that the powder is composed of nearly spherical shaped particles with size ranging from 3 - 12 nm (average size of 6.7 nm). The average crystallite size from TEM is about 2 times bigger in size than the crystallite size calculated from XRD data. HRTEM images obtained

for sample S_1 (Fig. 4b) shows clear lattice fringes of d = 0.312 nm corresponding to the (111) crystallographic plane of cubic ZnS.

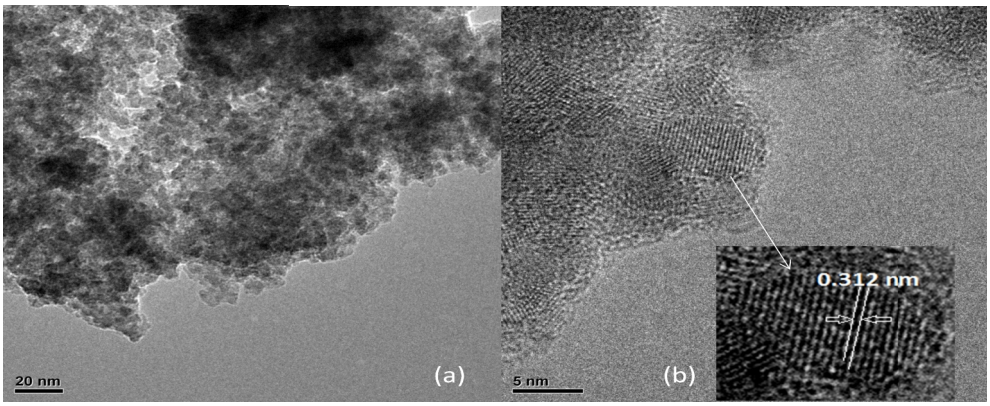

Fig. 4. The TEM image (a) and HRTEM image (b) of ZnS nanoparticles capped with CMC (sample S_1). Inset showing the value d-spacing for a single crystal in the (111) plane

3.3 Determination of ZnS/CMC Energy Band-Gap and Particle Size Using Effective Mass Approximation (EMA)

Fig. 5(I) shows the room temperature UV-Vis spectra of samples S_1, S_2 and S_3 respectively. The absorption peaks are located at 295 nm, 290 nm and 300 nm respectively. The spectra are similar to those obtained by [31] for ZnS:Mn^{2+} using similar spectrophotometer (JENWAY 6405 UV-Vis spectrophotometer).

Fig. 5(II) is the plot of the square of the absorption coefficient, $\alpha(h\nu)^2$ versus $h\nu$ $h\nu$ used to determine the energy band gaps for the three samples. The absorbance measurement data (A) were converted to transmittance using equations (2) and (3) as follows [32]:

$$\alpha = \frac{2.303A}{t} \tag{2}$$

$$\alpha = \frac{1}{t}\ln\left(\frac{1}{T}\right) \tag{3}$$

Equating (2) and (3) gives equation (4);

$$T = e^{-(2.303A)} \tag{4}$$

Secondly, the transmittance in equation (4) was normalized and the coefficient of absorption, $\alpha(h\nu)$ in equation (3) becomes:

$$\alpha(h\upsilon)^2 = \left[\frac{1}{t}\ln\left(\frac{1}{T_N}\right)\right]^2 \quad (5)$$

where t is the thickness of the film and T_N is the normalized transmittance.

Equation (5) was then substituted into the Tauc's formula (equation 6) for direct band gap semiconductor [32]:

$$\alpha(h\nu)^2 = \left(h\nu - E_g\right) \quad (6)$$

The plot of $\alpha\left(h\nu\right)^2$ versus $h\nu$ gave discontinuities at the transition energy of the sample in the plot. The minimum point in the discontinuity region where the value of $\alpha(h\nu)^2 = 0$ corresponds to the forbidden band gap energy $h\nu$ of the material. The obtained band gap energy gave small average particle sizes with band gap energies greater than 4.0 *e*V (Table 1). The energy band gaps are blue shifted from bulk ZnS (3.60 eV) [33]. It is clear from the blue shift in energy that quantum confinement of the electrons and holes has taken place [33].

Using the values of the band gap energies in Table 1, the average particle size of each sample was determined using the EMA [34]:

$$E_n = E_b + \frac{\hbar^2\pi^2}{2r^2}\left(\frac{1}{m_e^*} + \frac{1}{m_h^*}\right) - \frac{1.8e^2}{4\pi\varepsilon\varepsilon_0 r} - \frac{0.124e^4}{\hbar^2(4\pi\varepsilon\varepsilon_0)^2}\left(\frac{1}{m_e^*} + \frac{1}{m_h^*}\right)^{-1} \quad (7)$$

where E_n is the energy of nanoparticle, E_b is the energy of bulk ZnS (3.6 eV), m_e^* and m_h^* are the effective masses of electron and hole respectively, r is the radius of nanoparticle, e is electronic charge, ε and ε_o is the dielectric constant of the material and free space respectively. The effective masses used for calculation in this work are; $m_e^* = 0.23m_o$ and $m_h^* = 0.34m_o$ for electron and hole, respectively, while m_o is the electron rest mass [35].

The calculated results for particles size using EMA are shown in Table 1. The values of the average particle sizes calculated from XRD and EMA are slightly larger than the exciton Bohr radius (a_B ~ 2.5 nm) for ZnS, supporting week confinement regime [36]. The particle sizes calculated using EMA are comparable to the obtained crystal sizes from XRD patterns. It has been reported that EMA overestimates the size of particles smaller than 5.0 nm, but gives the true average particle size for larger particles size distribution [37-39]. Nevertheless, particle sizes determined using EMA are in good agreement with the crystallite sizes obtained from XRD pattern.

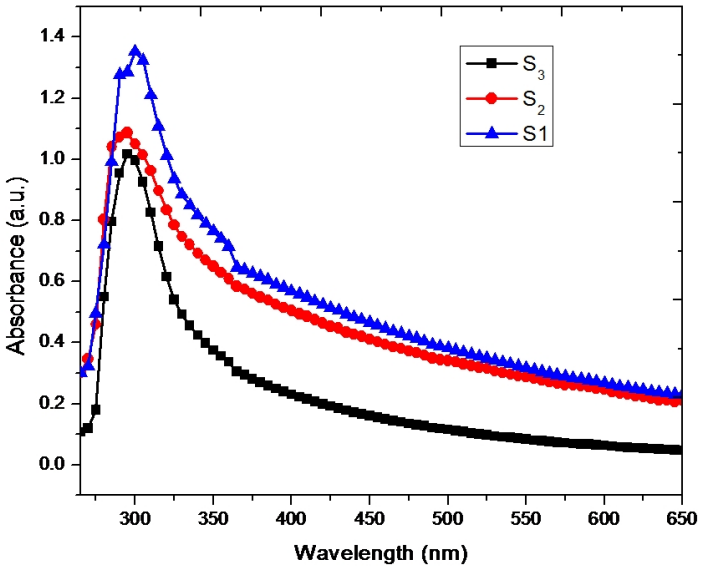

Fig. 5(I). Absorption spectra for S_1, S_2 and S_3 samples

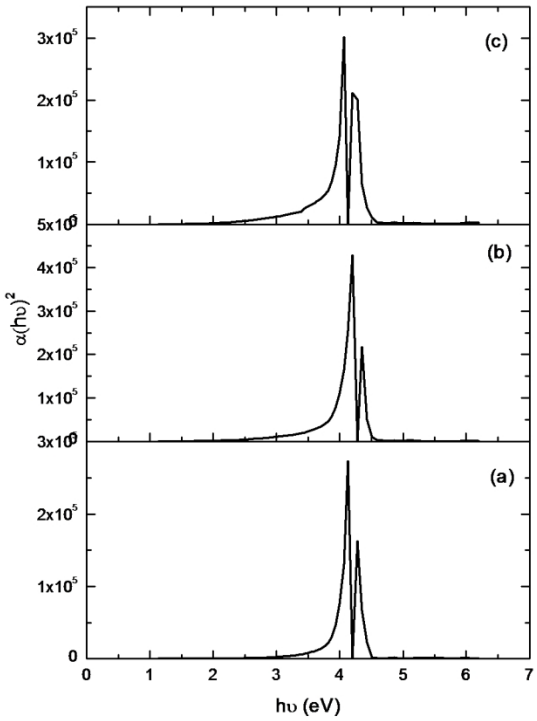

Fig. 5(II). Energy band gap for (a) S_3 (b) S_2 and (c) S_1 samples

3.4 Fourier Transform Infra-Red (FTIR) Analysis

Fourier Transform Infrared spectrum (FTIR) of the CMC used for capping ZnS nanoparticles and S_3 sample are shown Fig. 6(a) and Fig. 6(b), respectively. The FTIR spectrum of CMC (Fig. 6a) was used as standard to confirm the presence of the capping agent on the S_3 sample even after rigorous washing. From Fig. 6(b), the peak 480 cm^{-1} is assigned to the metal – oxygen bonds [40] while the peak positioned at 619 cm^{-1} originate from ZnS bond, possibly due to Zn-S stretching [41]. The vibration bond at 1001 cm^{-1} can be assigned to –CH-O-CH_2 vibration of ether groups [42]. Vibrational mode peak at 1126 can be assigned to the C – O stretching bond vibration. The absorption bands at 1770 cm^{-1}, and 3202 cm^{-1} are due to C=O and –OH stretching bands respectively of the carboxylic acid [41,43]. Also, the broad absorption band at 3416 is due to the stretching frequency of –OH group [44]. The symmetric and asymmetric modes of stretching vibration of carbonyl (COO^-) group at 1614 and 1446 cm^{-1}, respectively are observed [22,45,46]. Some of these peaks observed in Fig. 6(b) are also found in Fig. 5(a), though with a shift in energy toward higher vibrations. The existence of the carboxymethyl substituent (COO^{-1}, -CH_2 and –O-) group in Fig. 6(a) and Fig. 6(b) confirm the presence of the capping agent (sodium carboxymethyl cellulose, CMC) on ZnS nanoparticles [45]. The presence of CMC after rigorous washing of the colloidal nanoparticles suggests that CMC inhibit the growth of particle by electrostatic stabilization and/or steric hindrances.

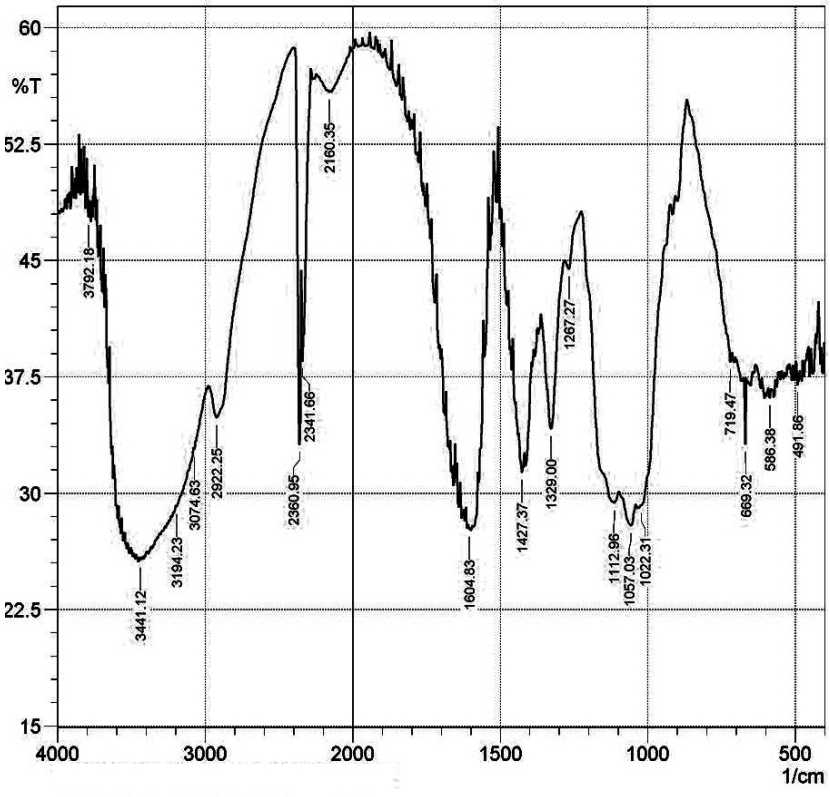

Fig. 6(a). FTIR spectrum of the CMC sample

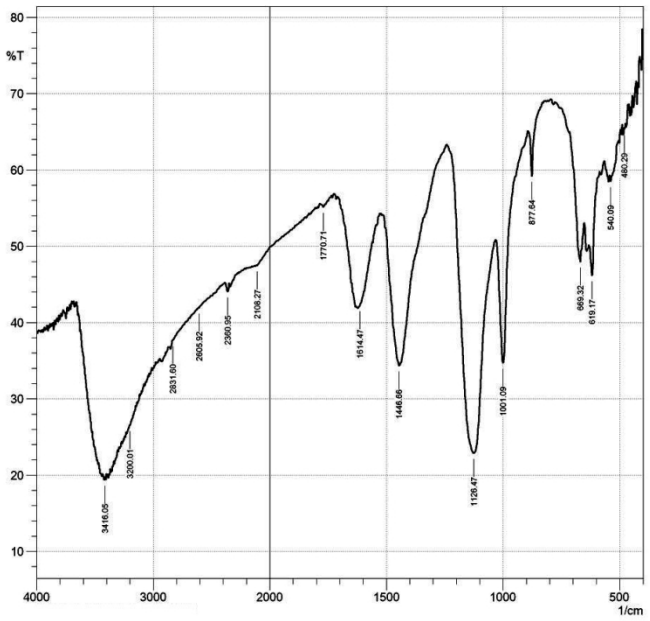

Fig. 6(b). FTIR spectrum of S_3 sample

3.5 Photoluminescence Emission and Excitation

Photoluminescence excitation spectra presented in Fig. 7(I) show the most prominent excitation bands at 285 nm and 330 nm and a broad excitation band at 360 – 450 nm. These bands correspond to the band-to-band, excitonic and impurity related excitation wavelengths of ZnS nanocrystals. Fig. 7, (II), (III) and (IV), show the emission spectra of S_1, S_2 and S_3 samples, respectively. All the spectra display single peaks centered at 442, 520 and 521 nm, respectively when the samples were excited with UV light at 320 nm wavelengths. The red shift of emission peaks position for samples S_2 and S_3 can be attributed to changes in the shape and dimension of the nanocrystals [28]. The emission spectrum of sample S_1 shows stronger PL intensity than the other samples. Luna-Martnez et al. [22] attributed similar observation to the relative larger amount of ZnS nanoparticles in CMC molecules. We attribute the enhanced photoluminescence emission intensity for sample S_1 to the combined defect related emissions of ZnS and its oxidants [i.e. ZnO or $Zn(OH)_2$] that coexist in the powdered sample as can be seen from the XRD pattern and TEM data. That is, the luminescence at 442 nm is caused by both oxygen vacancies as well as sulphur vacancies. The red shift in the PL spectrum can be attributed to an increase in the average size distribution of the ZnS crystallites and the disappearance of the ZnO particles due to a better passivation of nanocrystals surfaces by the CMC. The broadness of emission peaks of all samples synthesized in this work suggests larger particles size distribution [28]. This finding is supported by the average particle sizes obtained from SEM, TEM, and crystal size obtained from XRD.

For the ZnS nanocrystals, the observed blue and green PL emissions centered at 442 nm and 520 nm have been reported by [22] and others [11, 7] to be due to structural defects such as sulfur vacancies (V_s) and zinc interstitial (V_z). Specifically Luna-Martnez and co-

workers assigned the blue emission peak to surface V_s in a non-stoichiometry ZnS. Huang *et al*, [7] assigned the blue peak to surface V_s and the green peak to the transition between internal V_s and internal V_z. Surface sulfur vacancies have weak binding energies compared to the internal sulfur defects in nanocrystals [7]. Therefore, with increased CMC amount, the number of surface vacancies can be restrained; as a result the recombination between V_s donor levels with holes at the valence band becomes dominant. The observed peaks in the PL spectra of samples S_2 and S_3 are red shifted compared to other reports, this is likely due to the structural and particles size increase found for these samples.

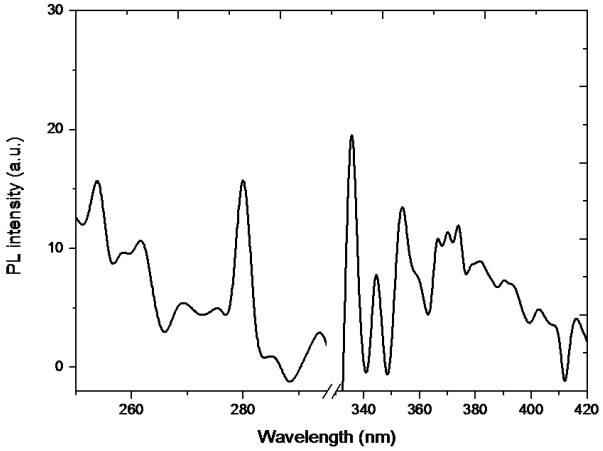

Fig. 7(I). Photoluminescence excitation spectra

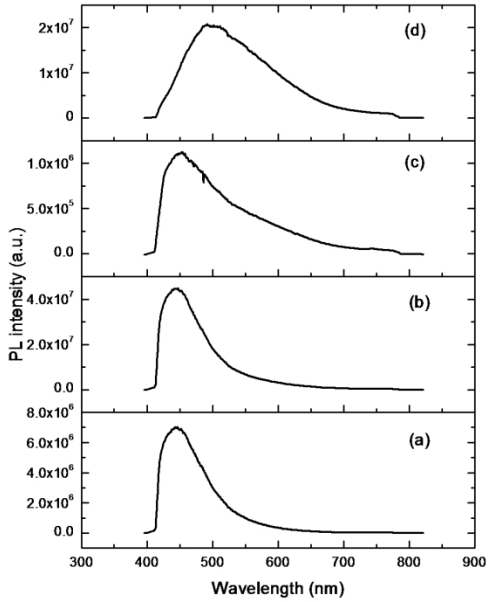

Fig. 7(II). Photoluminescence emission of sample S_1 at (a) 320 nm, (b) 345 nm, (c) 365 nm and (d) 394 nm excitations

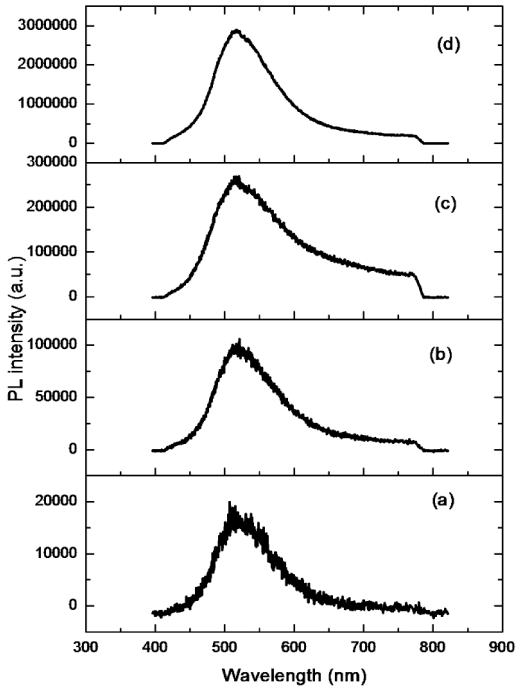

Fig. 7(III). Photoluminescence emission of sample S_2 at (a) 320 nm, (b) 345 nm, (c) 365 nm and (d) 394 nm excitations

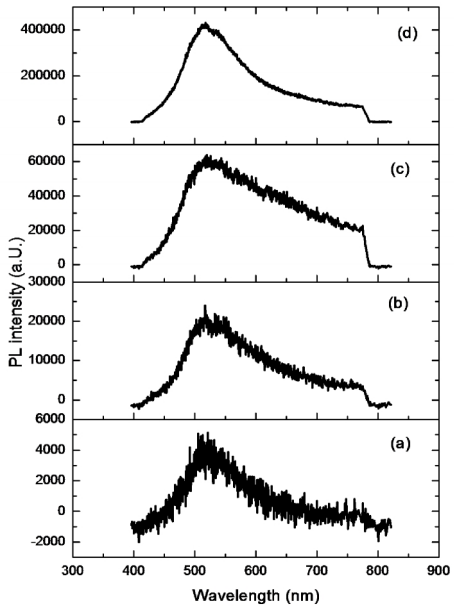

Fig. 7(IV). Photoluminescence emission of S_2 sample at (a) 320 nm, (b) 345 nm, (c) 365 nm and (d) 394 nm excitations

4. CONCLUSION

Zinc sulfide nanoparticles capped with CMC at different amount by volume was synthesized using precipitation method. The nanoparticles show structural degradation when they were kept for six months before characterization. ZnS sulfide capped with CMC at 1:1 (vol/vol) of nanoparticles-to-CMC ratio (S_1), show higher degradation, high emission intensity (with blue shift which is characteristic of surface state emission) and a mixed (small and larger) crystallite size distribution. The S_3 sample show better stability, a red shift in emission spectra and smaller mean crystal size distribution. The obtained mean particle size for all the samples was less than 30 nm indicating nanoparticles with weak quantum effect.

ACKNOWLEDGEMENTS

The authors wish to thank Dr Viana Bruno of Laboratorire de Chimie de la Matière Condensee de Paris, France for the photoluminescence analysis. Also, our gratitude goes to National Agency for Science and Engineering Infrastructure Abuja, Nigeria (NASENI) for funding part of this work.

COMPETING INTERESTS

Authors have declared that no competing interests exist.

REFERENCES

1. Hu H, Zhang W. Synthesis and Properties of Transition Metals and rare Earth Doped ZnS Nanoparticles. Opt. Mater. 2006;28:536–550.
2. Li GH, Su FH, Ma BS, Ding K, Xu SJ, Chen W. Photoluminescence of Doped ZnS nanoparticles under hydrostatic pressure. Phy. Stat. Sol. (B). 2004;241(14):3248-3254.
3. Bouvy C, Piret F, Marine W, Su BL. Preparation, photoluminescent properties and quantum size effect of ZnS nanoparticles at mesoporous silica CMI – 1. Chem. Phys. Lett. 2007;433:350–354.
4. Chatterjee A, Priyan A, Bhattacharya SC, Saha A. Differential growth and photoluminescence of ZnS nanocrystals with variation of surfactant molecules. Coll. Surf. A: Physicochem. Eng. Aspects. 2007;297:258–266.
5. Peng WQ, Cong GW, Qu SC, Wang ZG. Synthesis and Photoluminescence of ZnS:Cu Nanoparticles. Opt. Mater. 2006;29:213-317.
6. Mashfold B, Baldauf J, Nguyen T, Funston AM. Synthesis of Quantum Dot Doped Chalcogenide Glasses via Sol-gel Processing. J. Appl. Phys. 2011;109:094305.
7. Huang Q, Dong, D, Xu J, Zhang X, Zhang H, Li, L. White emitting ZnS nanocrystals: synthesis and spectrum characterization. Chin. Phys. Lett. 2010; 27, 5, 057306.
8. Sharma M, Kumar SOP. Photo-physical and morphological studies of organically passivated core-shell ZnS Nanoparticles. Dig. J. Nanomater. Biostructs.. 2010;3(4):189-197.
9. Bera D, Qian L, Tseng T, Holloway PH. Quantum dots and their multimodal applications: A Review. Materials. 2010; 3:226–2345.
10. Tachikawa S, Noguchi A, Tsuge T, Hara M, Odawara O, Wada H. Optical properties of ZnO nanoparticles capped with polymers. Materials. 2011;4:1132–1143.

11. Nirmala Jothi NS, Sagayaraj P. The influence of capping by TGA and PVP in modifying the structural, morphological, optical and thermal properties of ZnS nanoparticles. Arch. Appl. Sci. Res. 2012;4(2):1079–1090.
12. Hasanzadeh J, Shayesteh SF. Luminescence of doped CdS nanocrystals: effect of doping and capping agent. Optica Applicata 2012;XLI:4.
13. Zhu Z, Ma X, Qian X, Yin J. Preparation and characterization of polyvinyl alcohol-selenide nanocomposites at room temperature. J. Mater. Chem. 2002;12:663-666.
14. Murugadoss G, Rajamannan B, Ramasamy V. Synthesis and photoluminescence study of PVA-capped ZnS: Mn^{2+} nanoparticles. Digest Journal of Nanomaterials and Biostructures. 2010;5(2):339–345.
15. Onwudiwe DC, Ajibade, PA. ZnS, CdS and HgS Nanoparticles via Alkyl-Phenyl Dithiocarbomate Complexes as Single Source Precursors. Int. J. Mol. Sci. 2011;12,5535–5551.
16. Ehiaraj AS, Wu H, Gopal J. Synthesis and characterization of ultrasmall thioglycerol modified quantum dots. J. Chin. Chem. Soc. 2011;58(6):1-4.
17. Alvaro A, de Queiroz A, Mayler M, Demetrio AWS, Ecio JF. Modeling of ZnS quantum dots synthesis by DFT techniques. J. Mol. Struct. 2008;873:121–129.
18. Yang P, Bredol M. Surface passivation and photoluminescence of Mn-doped ZnS nanocrystals. Res. Lett. Mater. Sci. 2008;506065:1–5.
19. Qu SC, Zhou WH, Liu FQ, Chen NF, Wang ZG. Photoluminescence properties of Eu^{3+} - doped ZnS Nanocrystals prepared in a water/methanol solution. Appl. Phys. Lett. 2002;8(19):3605–3607.
20. Nath SS, Chakdav D, Gope G, Avasthi DK. Characterization of CdS and ZnS quantum dots prepared via chemical method on SBR latex. Azono J. Nanotechnol. 2008;4:1–6.
21. Sakulchaicheroen N, O'carroll DM, Herrera JE. Enhanced stability and dechlorination activity of pre-synthesis stabilized nanoscale FePd particles. J. Contam. Hydrol. 2010;118:117–127.
22. Luna-Martinez JF, Hernandez-uresti DB, Reyes- Melo ME, Guerrero-salazar CA, Gonzalez-Gonzales VA, Sepuiveda-Guzman S. Synthesis and optical characterization of ZnS – Sodium Carboxymethyl cellulose nanocomposite films, Carbohy. Poly. 2011;84:566–570.
23. Rachtanapun P, Suviyatem R. Value added of Durian Husks: Synthesis of carboxymethyl cellulose from Dunian Husk. Chiang Mai University, Thailand; 2008.
24. Starr KF. Microbial Implication of iron Nano Particles. M.Sc. Thesis, Aubun University Alabama; 2010.
25. Jiang D, Cao L, Lu W, Su, G, Qu H, Sun, Dong B. Synthesis and Luminescence properties of core/shell ZnS: Mn/ZnO nanoparticles. Nanoscale Res. Lett. 2008;4:78-83.
26. Seetawan U, Jugsujinda S, Seetawan T, Euvananont, Amornkitbamrung V. Effect of annealing Temperature on the Crystallography, Particle size and thermopower of bulk ZnO. Sol. State Sci. 2011;13:1599–1603.
27. Fang X, Zhai T, Gautam UK, Li L, Wu L, Bando Y, Golberg D. ZnS nanostructures: From synthesis to application. Prog. Mater. Sci. 2011;56:175-287.
28. Mehta SK, Kumar S, Chaudhary S, Bhasin KK. Effect of surfactant head groups on synthesis, growth and agglomeration behavior of ZnS nanoparticles. Nanoscale Res.Lett. 2009;4:1197-1208.
29. Rachtanapun P, Suriyatem R. Value added of Durian Husk: Synthesis of Carboxymethyl Cellulose from Durian Husk. Project Report, Chiang Mai University, Thailand; 2009.

30. Moosavi-Nasab M, Yousefi AR, Askari H, Bakhtiyari M. Fermentative Production and Characterization of Carboxymethyl Bacterial Cellulose using Data Syrup. World Acad. Sci. 2010;14:1480.
31. On–Uma N. Synthesis and characterization of Nanocrystalline ZnS: Mn^{2+} polyelectrolyte. M.Sc. Thesis, Mahidol University; 2005.
32. Chao S. Effect of growth temperature on the properties of ZnO thin films grown by radio-frequency magnetron sputtering. Transl. Electri. Electro. Mater. 2009;10(6):185 – 188.
33. Bol AA, Ferwerda J, Bergwerff JA, Meijerink A. Luminescence of Nanocrystalline $ZnS:Cu^{2+}$. J. Lumin. 2002;99:325-334.
34. Zhang JZ. Interfacial Charge Carrier Dynamics of Colloidal Semiconductor Nanoparticles. J. Phys. Chem. B. 2000;104:7239-7253.
35. Bhattacharjee B, Lu C. Effect of microwave power on the physical properties of carboxylic acid-coated Maganese-ion-doped Zinc Sulfide nanoparticles. J. Nanotechnol. Doi: 10.1155/2011/916750; 2011.
36. Tang H, Xu G, Weng L, Pan L, Wang L. Luminescence and PhotophysicalProperties of Colloidal ZnS Nanoparticles. Acta Materialia, 2004;52:1489-1494.
37. Wang Y, Herron N. Nanometer Semiconductor clusters materials synthesis, Quantum size effects and photophysical properties. J. Phys. Chem. 1991;95:525-532.
38. Marandi M, Taghavinia N, Iraj AZ, Mandevi. Fine particles of size of CdS Nanoparticles synthesized by a photochemical method. Nanotechnol. 2006;17:1230–1235.
39. Jamali Sh, Saievar-Iranized E, Shayestech SF. Synthesis, Optical and structural Characterization of CdS Nanoparticles. Int. J. Nanosci. & Nanotechnol. 2007;3:1.
40. Jeong JH, Kyoung H. Synthesis, crystal growth and photoluminescence properties of YAG: Eu^{3+} phosphors by High-Energy ball milling and solid state reaction. J. Phys. Chem. C; 2009.
41. Staurt B. Infrared Spectroscopy: Fundamentals and Applications. John Wiley and Sons, Ltd; 2004.
42. Kondo T. The assignment of IR absorption bands due to free hydroxyl groups in cellulose. Cellulose. 1997;4:281–292.
43. Brusau EV, Pedreggosa JC, Narda GE, Ayala EP, Oliveira EA. Vibrational and Thermal Study Hexaaquatrism (malonato) Dieuropium (III) Dihydrate. The J. Argentine Chem. Soc. 2004;92(1/3):43-52.
44. Rachtanapun P, Mulkara N. Pintajam N. Effects of sodium hydroxide concentration on mechanical properties of carbocymethyl cellulose films from waste of mulberry paper. 5^{th} International packaging congress and exhibition, November 22-24, 2007;Bayrakli-Izmir-Turkiye chamber of chemical engineers-ege branch, Turkey.
45. Pecsok RL, Shields LO, Cairns T. McWilliam IG. Modern Method of Chemical Analysis. New York: Willey; 1976.
46. Adnugraha MP, Marseno DW, Hayadi J. Synthesis and Characterization of Sodium Carboxymethyl Cellulose from Cavendish Banna Pseudo Stem (Musa Cavendishii LAMBERT). Carbohy. Poly. 2005;62:164–169.
47. Hatim ME, Xu L, Huang X, Li M, Chen K. Enhancement of Band edge Emission from $ZnS/Zn(OH)_2$ Quantum Dots. Chin. Phys. Lett. 2001;18(4):616–618.

48. Jindal Z, Verma NK. Effect of UV Radiation on the Photoluminescent Properties of Cu-doped ZnS Nanoparticles. Optoelectro. & Adv. Mater. – Rapid Communications. 2008;2(3):144-149.

Peer-review history:
The peer review history for this paper can be accessed here:
http://www.sciencedomain.org/review-history.php?iid=226&id=5&aid=1841